Team-based Robot Righting via Pushing and Shell Design

David L. McPherson Ronald S. Fearing

***Abstract*— The minimalist robot designs typically employed in swarms and teams can fall and get trapped when traversing irregular terrain. To protect against this contingency the design could add a specialized escape actuator, but each actuator drives up cost multiplicatively for the whole team. Instead, the emergency actuator can be found for free in the form of another teammate. Teammate pushing can be efficiently directed by careful shaping of the robot's exterior hull. This approach is illustrated by designing a shell for VelociRoACH robots that enables them to roll pronated comrades back onto their feet. The designed maneuver can be performed in open-loop with 87% success and an average time of 0.7 seconds.**

I. Introduction

Affordable teams of robots must be designed with an economy of actuators. While elegant minimalistic mechanics can mobilize the robot to traverse the whole state space (e.g. [19]), there will inevitably be states the robot cannot escape. For example, the lightweight design of the VelociRoACH [5] can dynamically explore irregular terrain, yet stumbling can trap the robot on its back [8] thereby eliminating all of its degrees of freedom (DoF). This contingency has caused previous designs [9][2] to add specialized actuators (and therefore, expense and weight). The present work demonstrates how to add actuators to the system only during the contingency and then reallocate them afterwards: teammates can serve as the assisting actuators.

While prior work has investigated modes of cooperative locomotion [1][15], they require permanently linking two robots together into an equivalent of one over-actuated robot. Moving teammates without permanent connections requires affecting through transient contact alone — a challenge that manipulation research [14][18][17][16] has wrestled with for decades. Indeed, the contact-based cooperative locomotion task contains both the manipulation task and its reciprocal: besides shaping a manipulator to move an object [13], cooperative locomotion must shape the object to be easily moved by a manipulator. Further, the "manipulator" in cooperative locomotion has minimistically few DoF requiring non-prehensile [11] approaches to manipulation. These focus on shape [13][3] and sliding [11][20] rather than actuator-intensive closure [14]. The present paper outlines this reciprocated design problem illustratively through the VelociRoACH un-pronation application.

This work is supported by the National Science Foundation under the National Robotics Initiative (Award CMMI-1427096) and the United States Army Research Laboratory under the Micro Autonomous Science and Technology Collaborative Technology Alliance

All authors are with the Department of Electrical Engineering and Computer Science, University of California, Berkeley {david.mcpherson, ronf}@eecs.berkeley.edu

Fig. 1: Frame sequence of RoACH team performing cooperative righting maneuver.

Section II-A discusses the co-design of the manipulator's and manipulandum's shape in the plane of movement. This shape can be chosen to ensure stable pushing contact throughout the maneuver. To proscribe the performance of the maneuver itself, the shape design problem shifts to the out-of-plane shape. This problem is motivated by overcoming gravitational potential energy barriers like in [7][6], but Section II-B argues that the work should be dispersed finely over a continuous push rather than concentrated into discrete transitions like in [7]. This argument results in a rounded shell that rolls like a wheel and is domed like a turtle shell [4]. This design's requirements and failure modes are analyzed in Section II-C, and experimentally tested in Section III-C. Testing on hardware demonstrated that the design succeeded in aligning (Sec. III-A) and righting the fallen robot quickly (average time of 0.7 seconds) and reliably (success rate of 87%).

II. Shell Design

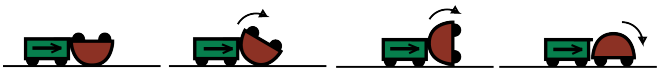

Fig. 2: Cooperative righting maneuver concept

The first imperative for contact-based cooperation is to ensure stable transfer of manipulation forces between teammates. In Section II-A, Reuleaux's method [12] shows that a rectangular footprint for the shells will align manipulator and manipulandum without closed loop control and allow for stable pushing. These pushing forces must be used to overcome the gravitational energy barriers that trap the pronated robot. Taking inspiration from domed turtle shell shapes, whose righting properties were studied by Domokos et al. [4], the locomotion-focused shell design simply translates the idea of the wheel into manipulator/manipulandum co-design (as seen in Fig. 2). An energetic analysis examines design tradeoffs in shrinking the height of the shell wheel into an ellipse in Section II-B. After choosing a shell shape, Section II-C examines failure modes and minimum requirements for

the friction and necessary pushing force using a Newtonian analysis.

A. Reuleaux's Analysis

The shell footprint will govern how the robot yaws (i.e. rotates about the vertical axis) when interacting with the environment. The footprint should be designed so that yaw will be passively stable throughout contact. Reuleaux's method [12] reveals that a rectangular footprint drives the robot to align with objects (esp. other teammates) it engages with, resulting in stable pushes. Fig. 3 shades areas corresponding to moment labels (green for clockwise rotation centers, a lighter red for counterclockwise rotation centers). Note that for the rectangle-rectangle contact the multilateral constraint rules out centers-of-rotation between the two contacts where the moment labels contradict each other (and is labeled a mixed darker shade).

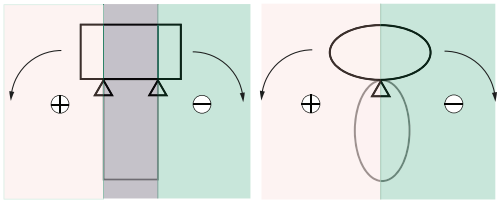

Fig. 3: Applying Reuleaux's method to contact constraints. The pink region marks the set of counterclockwise candidate rotation centers for the manipulated robot, while the green region marks the clockwise ones. The rectangular footprints have a zone stability where no rotation can occur.

The true stability is manifested when a second virtual finger is added via friction (assuming weight is distributed symmetrically) or the inertial pseudo-force. Drawing this added force on the diagram collapses the space of possible rotation centers (see Fig. 4).

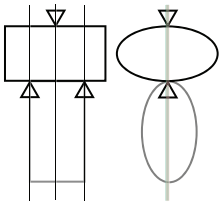

Fig. 4: Improved interaction stability between rectangular footprints over ellipsoidal footprints with added friction reaction force.

The prismatic shells have full force closure (with friction) in the yaw axis. In contrast, the ellipsoidal shells (the previous art for RoACH shells) still has infinitely many possible rotation centers: confined now to the line through both centers (in the best case) or the area between the centerlines if the pusher is even slightly misaligned. Therefore, by Reuleaux's method, the prismatic shells have a stable grasp while the ellipsoidal grasps are an unstable equilibrium.

Leading into these grasps, too, the prismatic shells are more stable. If the two rectangles are rotationally offset upon first contact, only one corner of the pusher will touch the prone robot. If the pronated robot's center is between this contacting corner and the opposite corner, then the prismatic shell will be pulled into a stable perpendicular configuration. In contrast, if the ellipsoidal shells are rotationally offset upon first contact, the pusher is deflected away from its compatriot and no grasp is achieved. This deflecting behavior was the original appeal of the ellipsoidal design in Li et. al's work [10], which referred to this effect as "terradynamic streamlining". For stable pushing, however, this contact avoidance is undesirable. A prismatic shell design will be anti-"terradynamically streamlined" and better for robust force transfer.

B. Lagrangian Analysis

After choosing a prismatic ground footprint, our shape design problem reduces to choosing the vertical cross-section. The problem for robot-righting is to overcome the gravitational potential energy well that keeps the robot prone (as discussed by Kessens [7]). Escaping this energy well will be accomplished by injecting work from the pushing robot and the ground friction. Assuming the friction force constrains the robot to roll without slip[1], the out-of-plane cross section's state dimension is reduced from two-space to the one-dimensional manifold parametrized by the roll angle θ:

$$L(\theta, \dot{\theta}) = T(\dot{\theta}, \theta) - U(\theta) = -U(\theta)$$

Where the analysis has been simplified by assuming a quasi-static interaction (i.e. kinetic energy $T(\dot{\theta}, \theta)$ is zero). The quasi-static equilibrium force equations for the horizontal axis show that the friction and pushing forces must have equal magnitudes. Therefore they form a moment couple $M = Fh$ where h is the height of the pushing robot and F is the force the pushing robot must provide. This exogenous torque (the equivalent of a force in the Lagrangian coordinate) produces the generalized Lagrangian equation of motion:

$$M = \frac{d}{dt}\frac{\partial L}{\partial \dot{\theta}} - \frac{\partial L}{\partial \theta} \tag{1}$$

$$= -\frac{\partial L}{\partial \theta} = \frac{dU}{d\theta} \tag{2}$$

The exogenous pushing force M required will equal the derivative of potential energy with respect to the generalized coordinate θ. The shell design should minimize this energy consumption, especially since the VelociRoACH platform was not optimized for torque production (instead being geared towards high velocities). Smoother potential energy surfaces (i.e. those with shallower slopes) will require less pushing force. Therefore, the shell design investigation is focused to the space of ellipses to avoid pronounced corners and their unnecessarily high $\frac{\partial U}{\partial \theta}$ concentrations.

Consider Fig. 5 where a, b are the ellipse's major and minor axes' lengths. The energy at a given tilt angle θ will be:

[1]this assumption will be examined in the next design section

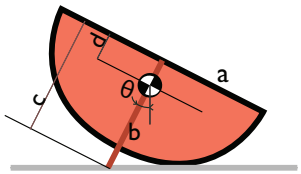

Fig. 5: Geometric diagram for energy analysis of a pivoting ellipse with major axis a, minor axis b, and center of gravity recessed d length along the minor axis.

$$U(\theta) = \begin{cases} mg(c(\theta) - d)\cos(\theta), \text{if } \theta < \frac{\pi}{2} \\ mg(a\sin(\theta) - d\cos(\theta)), \text{if } \frac{\pi}{2} \leq \theta < \frac{\pi}{2} + \tan^{-1}(\frac{d}{a}) \end{cases} \tag{3}$$

where c is the minor-axis intercept of the unique tangent line to the semi-ellipse with angle θ (this tangent defines the ground contact point):

$$c(\theta) \doteq \sqrt{a^2\tan^2(\theta) + b^2} \tag{4}$$

This energy landscape is plotted in figure 6a. The instantaneous change in energy the manipulating robot must provide for manipulation and rotation θ is:

$$\frac{dU}{d\theta} = \begin{cases} mg((a^2 - b^2)\frac{\sin(\theta)}{\sqrt{a^2\tan^2(\theta)+b^2}} + d\sin(\theta)), \text{if } \theta < \frac{\pi}{2} \\ mg(a\cos(\theta) + d\sin(\theta)), \text{if } \frac{\pi}{2} \leq \theta < \frac{\pi}{2} + \tan^{-1}(\frac{d}{a}) \end{cases} \tag{5}$$

This energy differential over position describes how much work must be performed which is equivalent to requisite push force (shown in equation 2). Fig. 6b plots this energy differential for a circle and ellipse that will later be tested in Section III-B.

Note that the maximum force for pushing a circle is non-decreasing and is maximum at $\theta = \pi/2$. In contrast, the maximum force for pushing an ellipse is much larger and occurs in the middle of the pushing maneuver. This larger energy requisite manifests in experiments as significantly slower pushing maneuvers when operating on ellipses in Section III-B. Therefore, within the space of ellipses, the circle is optimal for minimizing peak pushing force. For force-limited robotic platforms, like the VelociRoACH, this is a crucial optimality metric. The VelociRoACH design focuses on compactness, and adding a taller shell detracts from this strength. For application-ready robots, the design must balance these competing objectives.

C. Newtonian Analysis

Even the energetically-favorable circular prismatic shell can fail. For this pushing maneuver to succeed, both "fingers" must have sufficient force capacity: both the compatriot robot's push and the ground's friction force. These can be readily obtained by a quasi-static Newtonian analysis.

Extracting the equilibrium equations from the free-body diagram in Fig. 7 produces:

$$F = P \tag{6}$$
$$N = mg + B \tag{7}$$
$$0 = Pd\cos(\theta) + F(r - d\cos(\theta)) - Nd\sin(\theta) - B(r - d\sin(\theta)) \tag{8}$$

where P is the pushing force from the compatriot robot, B is the friction along the robot-robot contact surface, N is the ground reaction force, and F is the ground friction. Experimental constants (like the friction coefficients μ or h) are described in Table I.

Assuming the prone robot's shell is sliding along the compatriot robot:

$$B = \mu P \tag{9}$$

1) Push Force Requisite: Manipulating equation 8 and substituting (in order) Eqs. 6, 7, 9

$$0 = Pr - Nd\sin(\theta) - B(r - d\sin(\theta)) \tag{10}$$
$$= (P - B)r - mgd\sin(\theta) \tag{11}$$
$$= (1 - \mu)Pr - mgd\sin(\theta) \tag{12}$$

Solving for P yields:

$$P = \frac{mg}{1 - \mu}\frac{d}{r}\sin(\theta) \tag{13}$$

Which means that the pushing robot needs to be able to apply at least the maximum push force required throughout the manipulation:

$$\text{push capacity} \geq P_{max} = \max_{\theta} \frac{mg}{1 - \mu}\frac{d}{r}\sin(\theta) \tag{14}$$
$$= \frac{mg}{1 - \mu}\frac{d}{r} \tag{15}$$

Note that any friction between the pusher's front surface and the pronated robot's shell increases the required push force. The requisite push force goes to infinity as μ approaches unity. Therefore, the friction between the two shells must be kept as low as possible or a stronger teammate will be needed.

2) Friction Requisite: This analysis examines where the rolling-without-slip assumption breaks. This breaking point will be on the border of the friction cone described by:

$$F \leq hN \tag{16}$$

where h is the friction coefficient between the pronated shell and the ground. Substituting equation 6 into the left-hand side of equation 16 and equation 7 into the right-hand side (along with equation 9) yields:

$$P \leq \frac{hmg}{1 - h\mu} \quad \forall\theta \tag{17}$$

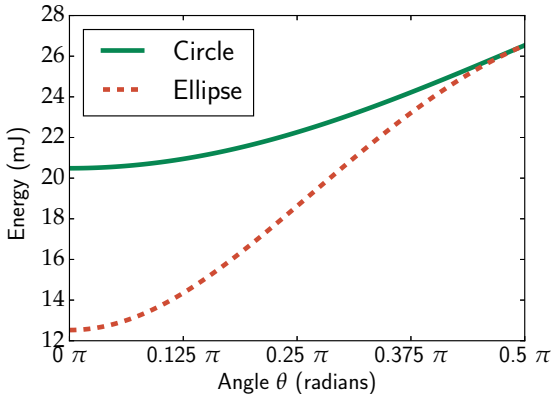

(a) Potential energy landscape plotted as a function of the manipulated robot's angle as described in equation 3.

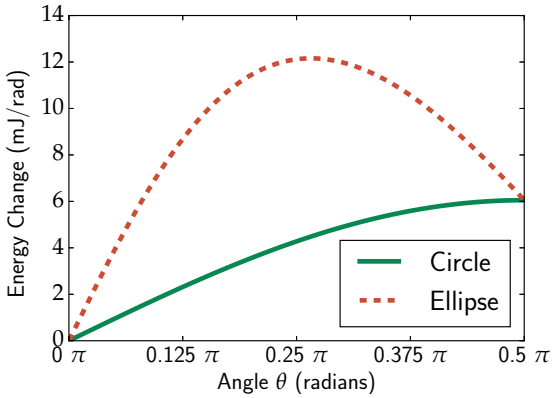

(b) Requisite push force $M = \frac{dU}{d\theta}$ plotted against manipulated robot's angle as described in equation 5.

Fig. 6: Energetic comparison of circular and elliptical shell cross-sections with $a = 5.0cm$, $b = 3.5cm$, $d = 1.14cm$.

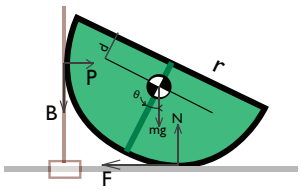

Fig. 7: Freebody diagram for quasi-static Newtonian analysis.

The tightest bound will be at the θ when push force is maximized P_{max}:

$$P_{max} = \frac{mg}{1-\mu}\frac{d}{r} \leq \frac{hmg}{1-h\mu} \tag{18}$$

$$\frac{1}{1-\mu}\frac{d}{r} \leq \frac{h}{1-h\mu} \tag{19}$$

assuming the shell-shell contact is frictionless reduces the requirement on the shell-ground contact to:

$$\frac{d}{r} \leq h \tag{20}$$

If the ground friction is insufficient the prone robot will only roll up to a critical angle θ_{break}. At that point the friction constraint is exactly met, the prone robot will begin to slide, and any further pushing will only result in sliding instead of rolling. To avoid this failure mode, a Santoprene tire is added at both ends of the robot shell, thereby boosting shell-ground friction coefficent[2] h (from 0.26 to 1.07) while leaving a subsection of the shell smooth for low friction shell-shell contacts μ.

III. Empirical Validation of Shell Design

The VelociRoACH is a Robotic Autonomous Crawling Hexapod (RoACH) experimental platform designed for high velocity running through its elegant minimal hardware design [5]. Due to its low cost and rapid manufacturing process, teams of RoACHes are a pragmatic platform for investigating multi-robot maneuvers [1]. It is powered by a single 3.7V 300mAh LiPo battery (Lectron Pro) and two 7mm, 3.3Ω coreless brushed DC motors.

This work equips the VelociRoACH with a shell to test the design principles extracted in Sections II-A, II-B, and II-C: rectangular footprints for alignability, taller shells for smoother energy landscapes, and boosted traction materials. The shell is vacuum-formed out of 15mm polycarbonate and attached to the robot via a neodymium magnet mount. The robot and shell together weight 54.1 grams (see Table I for the rest of the robot constants used in the analyses).

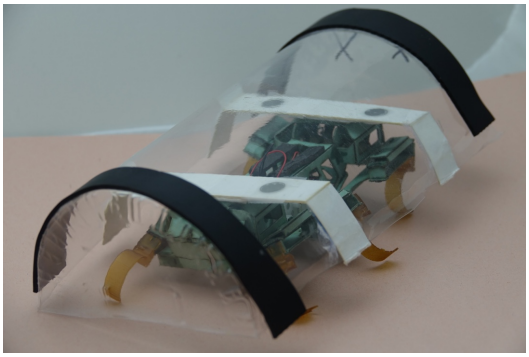

Fig. 8: VelociRoACH equipped with Roll Manipulation Shell (designed in Section II).

The robot controls its legs to track a 10Hz gait with no added steering; all yaw alignment will be through passive shell mechanics. This gait runs over a foam substrate with coefficients of friction h (recorded in Table I) for a fixed two second duration. The maneuver's performance is recorded and the success of the roll is assessed after the two seconds have elapsed.

The main design (circular shell with rubberized strips) and experimental condition (orthogonally aligned with manip-

[2]All friction coefficients were measured by placing the material on an incline and finding the minimum slope at which the static friction between the materials is overcome by gravity and starts to slip.

TABLE I: Physical Parameters of VelociRoACH and Shell

Parameter name	Symbol	Value
Body mass	m_b	54.1 g
Overall width, depth, height	(w, h)	$(10, 19, 10)$ cm
Shell circular radius	r	5.0 cm
Shell major, minor axis radius	(r, b)	$(5.0, 3.5)$ cm
Shell center offset height	d_{circle}	11.4 mm
	$d_{ellipse}$	7.27 mm
Shell-shell contact friction	μ	0.52
Shell-ground contact friction	h	0.26
...with rubberized strips on shell	$h_{rubberized}$	1.07

ulandum) were tested the most and compared to all three variants discussed below. Therefore when reading the below experimental results tables, the noise inherent in the lower trial resolutions will be ignored when noting trends.

A. Footprint Alignment

As analyzed in Section II-A via Reuleaux's method, robots with the prismatic design (rectangular footprint) will self-align when pressed together. When initialized with alignment (i.e. zero degree offset) the shell design successfully executed the righting maneuver 26 of 30 trials. When initialized with 30 degree, 45 degree, or 60 degree offsets the alignment succeeded in 5/5, 5/5 and 2/5 trials respectively. Therefore, past a 45 degree offset the self-alignability of the shells drops off, instead yawing the robots into the parallel (non-engaged) configuration.

TABLE II: Passive Mechanical Alignment of Rectangular versus Elliptical Footprints

Top View	Condition Description	Successes
	Prism, Straight (0 degree) Alignment	26/30 (87%)
	Prism, Scant (30 degree) Alignment	5/5 (100%)
	Prism, Scant (45 degree) Alignment	5/5 (100%)
	Prism, Scant (60 degree) Alignment	2/5 (40%)
	Ellpisoidal, Straight (0 degree)	0/5 (0%)

Note that although the straight alignment experiments have a lower percentage than the 30 and 45 degree alignments, this difference is within the $\pm 20\%$ tolerance for a five trial measurement.

The maneuver was then tested with elliptical footprints. Even when initialized aligned, the pusher deflected away from the target robot immediately upon contact (successful alignment in 0/10 trials). Contact-avoiding rounded footprints like the ellipse (what [10] would call "terradynamically streamlined") should be avoided for cooperative locomotion shell designs. Cooperative locomotion designs need to stably couple teammates' forces, so *shell designers should be mindful of the alignment effects of flat versus rounded surfaces*.

B. Cross-section Height: Circular versus Elliptical

The choice for a circular cross-section shape from Section II-B proved to perform 20% faster in experiments (see Fig. 9) than the elliptical design. The larger requisite push forces will be the bottleneck for the force-limited VelociRoACH team, and this strain is reflected in longer righting times and fewer successes. *Cooperative locomotion designers should smooth out the energy landscape (by smoothing out shapes along the plane of motion) to improve maneuver performance*.

TABLE III: Experiments Comparing Circular and Elliptical Prismatic Shell Cross Sections

Side View	Condition Description	Successes	Average Time (ms)
	Semi-circular Prism	26/30 (87%)	672 ms
	Semi-elliptical Prism	15/20 (75%)	817 ms

C. Ground Friction Requisite

As shown in equation 19 a minimum shell-ground friction coefficient is necessary to successfully perform a quasi-static flip. This requirement was confirmed in experiment, by varying the friction coefficient using the added tractive strips made of Santoprene rubber. The successful design condition discussed above (with the 26/30 success rate) used Santoprene strips. When these strips were removed the bare plastic failed to grip the ground and 5/5 flip attempts failed. This manifested as 3 out of 5 pushes failing due to the prone robot skittering away from the pusher (illustrated in Fig. 10), and 2 out of 5 pushes failing after the prone robot twisted (in yaw) away from the push.

TABLE IV: Experimental Results Demonstrating Importance of Ground Friction

Side View	Condition Description	Successes	Friction Requirement $\frac{h}{1-h\mu} \geq \frac{1}{1-\mu}\frac{d}{r}$ (equation 19)
	Rubberized	26/30 (87%)	$2.4 \geq 0.475$
	No-rubber	0/5 (0%)	$0.3 < 0.475$

Contact-based locomotion designers must be judicious not only with the surface's shape, but also its material properties (in this case, friction).

IV. Conclusion and Future Directions

We have shaped a robot shell through analysis and validated its efficient and reliable success on the VelociRoACH platform: the maneuver takes 0.7 seconds on average with an 87% success rate. Thus teamwork can right a fallen robot if robot shape is carefully designed. Shaping the robot hull simultaneously shapes the force landscape experienced between contacting robots. This force landscape can be used both to guide robots to stably lock together (like in Section II-A) and also to push robots up and away (like in Section II-B). Future developments should similarly be mindful of robot shape and considerate of how it can be employed to design cooperative maneuvers. The analyses from Sections II-B and II-C could be extended to interrogate the addition of dynamic effects — perhaps even harnessing them to augment the friction reaction force and strengthen the rolling moment couple. That moment couple could be also modulated by repositioning the pushing force from a reshaped "manipulator"-robot (possibly adapting the techniques of [13]).

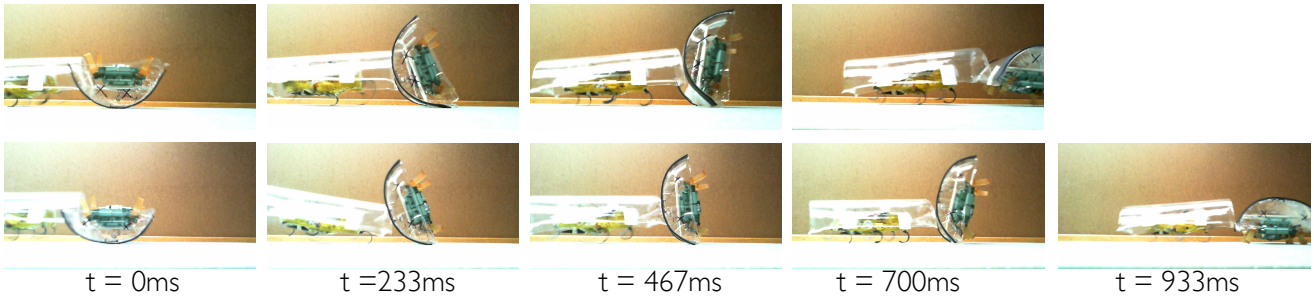

Fig. 9: Frame sequence of RoACH team performing cooperative righting maneuver with circular and elliptical shell cross-sections. Note the 20% slower maneuver completion rate for the elliptical design explained by the greater force requirements in Section II-B.

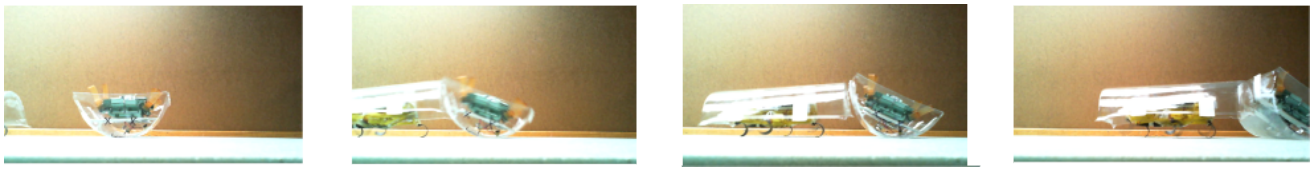

Fig. 10: Frame sequence of RoACH team failing to perform cooperative righting maneuver on styrofoam substrate due to insufficient ground-shell friction .

Beyond its proven capability to temporarily supplement lost DoF, shaping robots for cooperative pushing may enable adding DoF the robots never had. The manipulated robot could be reshaped to have energetically favorable capture regions [8] that allow it to be pitched upwards to scramble into a chimney or over a stair. Alternatively, robots could be hoisted upwards onto that stair by teammates shaped into ramps. A wide vista of design possibility opens up when understanding the robot hull not merely as a container for actuators and processors but as a means for manipulation.

Acknowledgements

Many thanks to Carlos Casarez for his indispensable advice on experimental design and analyses as well as general direction on where to take this project.

References

[1] Carlos S Casarez and Ronald S Fearing. Step climbing cooperation primitives for legged robots with a reversible connection. In *International Conference on Robotics and Automation (ICRA)*, pages 3791–3798, 2016.

[2] Carlos S Casarez and Ronald S Fearing. Dynamic terrestrial self-righting with a minimal tail. In *IEEE/RSJ International Conference on Intelligent Robots and Systems (IROS)*, 2017.

[3] Nikhil Chavan Dafle, Alberto Rodriguez, Robert Paolini, Bowei Tang, Siddhartha S Srinivasa, Michael Erdmann, Matthew T Mason, Ivan Lundberg, Harald Staab, and Thomas Fuhlbrigge. Extrinsic dexterity: In-hand manipulation with external forces. In *International Conference on Robotics and Automation (ICRA)*, pages 1578–1585, 2014.

[4] Gábor Domokos and Péter L Várkonyi. Geometry and self-righting of turtles. *Proceedings of the Royal Society of London B: Biological Sciences*, 275(1630):11–17, 2008.

[5] D. W. Haldane, K. C. Peterson, F. L. Garcia Bermudez, and R. S. Fearing. Animal-inspired design and aerodynamic stabilization of a hexapedal millirobot. In *IEEE International Conference on Robotics and Automation*, pages 3279–3286, May 2013.

[6] Chad C Kessens, Craig T Lennon, and Jason Collins. A metric for self-rightability and understanding its relationship to simple morphologies. In *IEEE/RSJ International Conference on Intelligent Robots and Systems (IROS)*, pages 3699–3704, 2014.

[7] Chad C Kessens, Daniel C Smith, and Philip R Osteen. A framework for autonomous self-righting of a generic robot on sloped planar surfaces. In *International Conference on Robotics and Automation (ICRA)*, pages 4724–4729, 2012.

[8] David J Kriegman. Let them fall where they may: Capture regions of curved objects and polyhedra. *The International Journal of Robotics Research*, 16(4):448–472, 1997.

[9] Chen Li, Chad C Kessens, Austin Young, Ronald S Fearing, and Robert J Full. Cockroach-inspired winged robot reveals principles of ground-based dynamic self-righting. In *IEEE/RSJ International Conference on Intelligent Robots and Systems (IROS)*, pages 2128–2134, 2016.

[10] Chen Li, Andrew O Pullin, Duncan W Haldane, Han K Lam, Ronald S Fearing, and Robert J Full. Terradynamically streamlined shapes in animals and robots enhance traversability through densely cluttered terrain. *Bioinspiration & Biomimetics*, 10(4):046003, 2015.

[11] Kevin M Lynch and Matthew T Mason. Dynamic nonprehensile manipulation: Controllability, planning, and experiments. *The International Journal of Robotics Research*, 18(1):64–92, 1999.

[12] Franz Reuleaux. *Theoretische Kinematik: Grundzüge einer Theorie des Maschinenwesens*. Braunschweig, F Vieweg und Sohn, 1875.

[13] Alberto Rodriguez and Matthew T Mason. Effector form design for 1dof planar actuation. In *IEEE International Conference on Robotics and Automation (ICRA)*, pages 349–356, 2013.

[14] Daniela Rus, Bruce Donald, and Jim Jennings. Moving furniture with teams of autonomous robots. In *IEEE/RSJ International Conference on Intelligent Robots and Systems*, volume 1, pages 235–242, 1995.

[15] TaeWon Seo, Carlos S Casarez, and Ronald S Fearing. High-rate controlled turning with a pair of miniature legged robots. In *International Conference on Robotics and Automation (ICRA)*, pages 5962–5968. IEEE, 2017.

[16] Peng Song and Vijay Kumar. A potential field based approach to multi-robot manipulation. In *International Conference on Robotics and Automation*, volume 2, pages 1217–1222, 2002.

[17] J Spletzer, Aveek K Das, Rafael Fierro, Camillo J Taylor, Vijay Kumar, and James P Ostrowski. Cooperative localization and control for multi-robot manipulation. In *IEEE/RSJ International Conference on Intelligent Robots and Systems*, volume 2, pages 631–636, 2001.

[18] Thomas G Sugar and Vijay Kumar. Control of cooperating mobile manipulators. *IEEE Transactions on robotics and automation*, 18(1):94–103, 2002.

[19] David Zarrouk and Ronald S Fearing. 1star, a one-actuator steerable robot. In *International Conference on Robotics and Automation (ICRA)*, pages 2569–2569. IEEE, 2014.

[20] Mike Tao Zhang and Ken Goldberg. Gripper point contacts for part alignment. *IEEE Transactions on Robotics and Automation*, 18(6):902–910, 2002.